



Article

Comparative Assessment of Shear Demand for RC Beam-Column Joints under Earthquake Loading

Angelo Marchisella *  and Giovanni Muciaccia 

Department of Civil and Environmental Engineering, Politecnico di Milano, 20133 Milano, Italy;
giovanni.muciaccia@polimi.it

* Correspondence: angelo.marchisella@polimi.it

Abstract: This paper focuses on the evaluation of bi-axial shear demand for reinforced concrete (RC) beam–column joints assuming: (i) the SPEAR frame as a benchmark; and (ii) different structural analysis methods which share the same seismic input. A numerical model was implemented using lumped plasticity. The joints were modeled as rigid offsets of beams and columns. The shear demand at a joint is evaluated as a post-process of the beam’s nodal moment. The discussion focuses on the differences between the estimated shear demand considering modal-response-spectrum analysis (MRSa), non-linear static analysis (NLSA) and non-linear time history (NLTH). Strength assessment of joints is discussed as well. Significant strength differences were recognized by using different building codes targeted to existing structures which, in general, behaved on the safe side. The elliptical shear strength domain resulted in being conservative when compared to NLTH shear demand orbits. NLSA, using modal combination, proved to estimate the larger shear demand with respect to MRSa and NLTH.

Keywords: SPEAR; RC beam-column joint; pushover



Citation: Marchisella, A.; Muciaccia, G. Comparative Assessment of Shear Demand for RC Beam-Column Joints under Earthquake Loading. *Appl. Sci.* **2022**, *12*, 7153. <https://doi.org/10.3390/app12147153>

Academic Editor: Maria Favvata

Received: 20 June 2022

Accepted: 13 July 2022

Published: 15 July 2022

Publisher’s Note: MDPI stays neutral with regard to jurisdictional claims in published maps and institutional affiliations.



Copyright: © 2022 by the authors. Licensee MDPI, Basel, Switzerland. This article is an open access article distributed under the terms and conditions of the Creative Commons Attribution (CC BY) license (<https://creativecommons.org/licenses/by/4.0/>).

1. Introduction

Post-earthquakes surveys revealed that beam–column joint failure is recurrent in RC buildings showing structural deficiencies such as inadequate joint reinforcement [1]. When a beam–column joint fails prematurely, the RC frame is both not able to sustain significant displacement demand and, eventually, loses its gravity load carrying capacity because of the buckling of column reinforcement [2].

The stress state of a beam–column joint is prevalently characterized by shear developed at the boundaries of the joint and at the interfaces between the joint concrete and the beam or column reinforcement [3]. Given its shear nature, design check is based on equilibrium between shear demand and shear strength [4]. Nonetheless, compatible models, defining the shear stress vs shear distortion constitutive law, are used in more sophisticated numerical applications [5].

According to Mohele [6], a beam column joint is defined as that portion of the column within the depth of the deepest beam that frames into the column. This definition implies that more than one beam can frame into the column and, consequently, force input should be considered bi-axial.

This paper focuses on the evaluation of bi-axial shear demand for beam–column joints, comparing different numerical methods to carry out seismic structural analysis. The selected benchmark structure is the SPEAR building [7]. First, the definition of joint shear demand and joint shear strength are summarized in the section titled “Fundamentals of RC beam–column joint”. Second, the section “Numerical study” presents the SPEAR frame by recalling the associated literature; details of the implemented numerical models are given as well. Third, the section “Results and Discussion” focuses on the shear demand at beam–column joints, highlighting the differences between modal-response-spectrum analysis,

non-linear-static-analysis and non-linear-time-history. Strength assessment according to building codes targeted to existing structures is discussed as well. Finally, some conclusions summarize the work.

2. Fundamentals of RC Beam-Column Joints

2.1. Joint Shear Demand

Considering an RC seismic primary frame such as the one shown in the Figure 1, a beam–column joint panel is defined as the zone where both the beam and column converge. A remarkable definition of the joint shear demand (V_j) is due to Paulay and Priestley [8], who assumed the joint panel as a continuous part of the column (the same considerations apply if it is considered as a part of the beam). When the diagram of bending moments are characterized by a seismic prevalent condition, a sign inversion is needed, passing from the top face to the bottom face of the joint panel. In this regard, V_j can be defined as follows, by considering it as the gradient of the bending moment within the beam depth:

$$V_{jh} = \frac{V_c(H - h_b)}{h_b}, \tag{1}$$

where V_c is the column shear, H is the distance between the column’s contraflexure points, h_b is the beam depth. As a result, by considering a common value of 3 m for H and 0.30 for h_b , the ratio V_{jh}/V_c amounts to 9, roughly suggesting that the shear demand in the beam–column joint has a different order of magnitude with respect to shear force either in the column or in the beam. Different results have been suggested by Paulay [8], who claimed the occurrence of a reduced gradient. In fact, V_{jh}/V_c was supposed to vary from four to six. Similarly, Mohele [6] suggested V_{jh}/V_c ranging from three to five for interior joints and half of those values for the exterior.

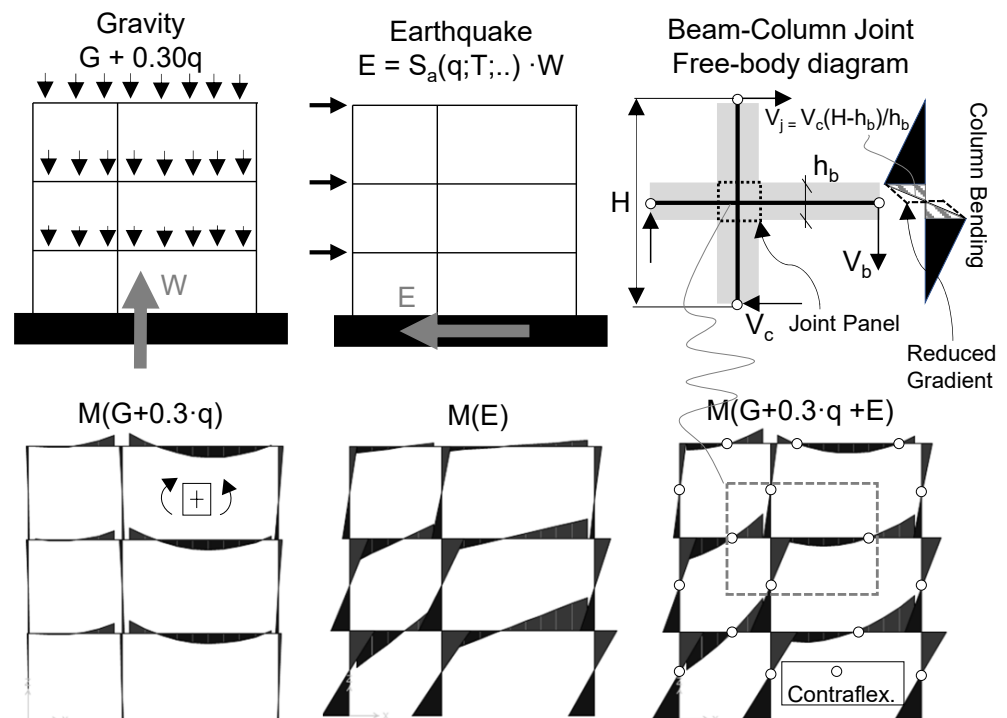


Figure 1. Beam–column joint definition for a planar moment-resisting frame under gravity and lateral forces. (Notes. The diagram of bending moment (M) are obtained from a simplified 2D analysis carried out on SPEAR frame).

The conventional definition of V_{jh} , widely adopted in design codes, is shown in Figure 2a. An interior beam–column joint is considered when the hogging moment acts on the right beam. After cutting with a horizontal plane, the horizontal free-body equilibrium requires:

$$V_{jh} = T_R + C_L - V_c, \tag{2}$$

where T_R is the tensile force of the top reinforcement on the right part, C_L is the result of compression stresses on the left part. This study assumes neglecting V_c in Equation (2). Such an assumption will always result in being conservative as long as the seismic condition is dominant for the bending moment diagram.

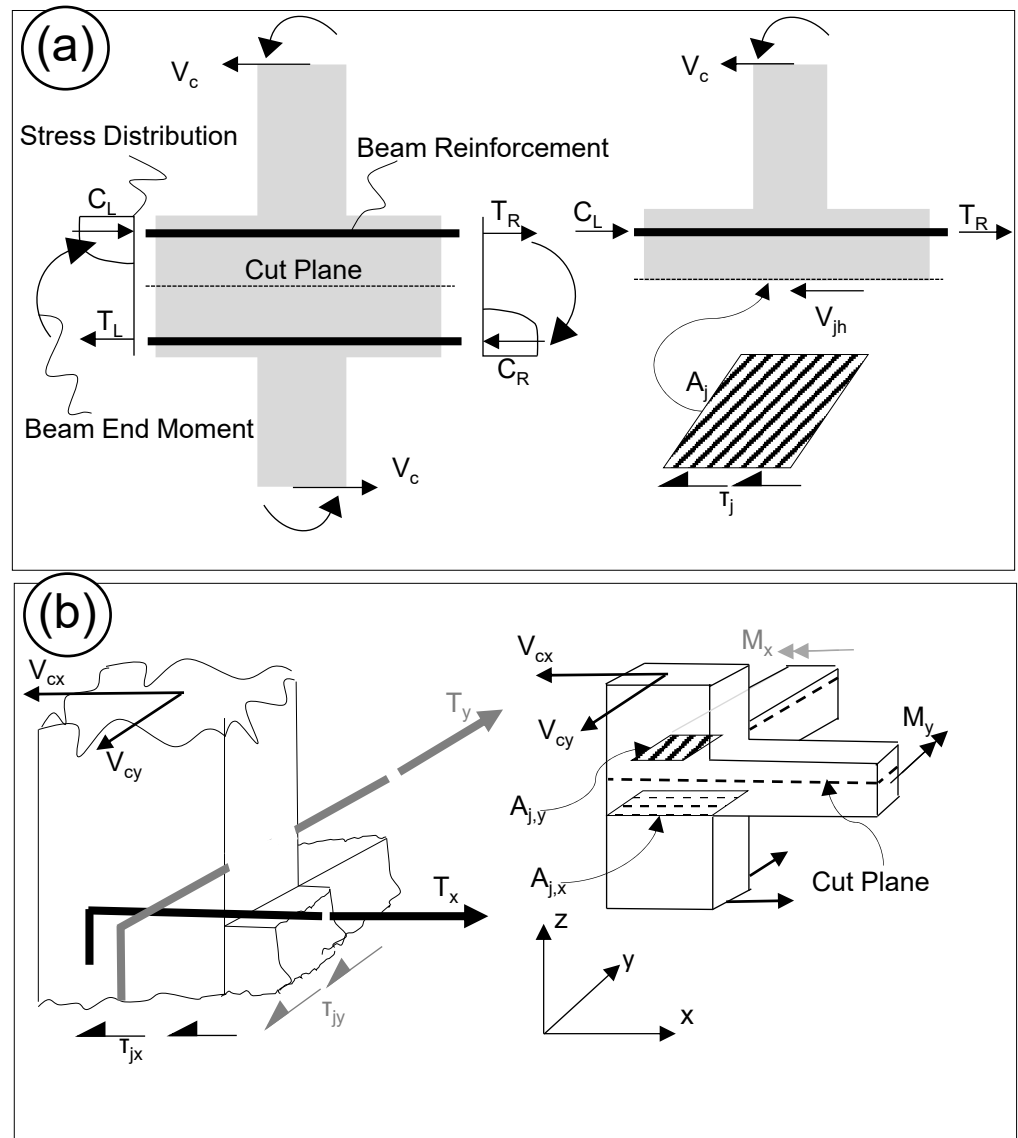


Figure 2. Horizontal joint shear (V_{jh}) definition: (a) Case of a 2D interior joint; (b) 3D corner joint.

A similar definition can apply, considering the case of a bi-dimensional joint as the one shown in Figure 2b. In this case, Equation (2) should apply both in x-z and y-z planes.

Frequently, shear stresses are used instead of shear forces. The definition is given as follows:

$$\tau_j = \frac{V_{jh}}{A_j}, \tag{3}$$

where A_j is the horizontal projection of the joint area.

According to ACI318 [9], the forces T_R and C_L , in Equation (2), should be calculated either from: (i) the maximum moments transferred between the beam and column as determined from factored-load analysis for beam–column joints with continuous beams in the direction of joint shear considered; or (ii) from the beam nominal moments strength possibly with overstrength. The latter is intended to account for: (a) the actual yield stress of a typical reinforcing bar being commonly 10 to 25% higher than the nominal value; and (b) the reinforcing bars strain hardening at member displacements only slightly larger than the yield rotation. EC8 [10] and ACI352 [11], specifying an overstrength factor (γ_{Rd}) equal to 1.20 and 1.25, respectively. As an example, by defining A_s as the area of the beam reinforcement anchored within the joint and f_y the yielding stress, the yielding force (T_y) can be written as follows:

$$T_y = A_s f_y \gamma_{Rd}. \quad (4)$$

2.2. Joint Shear Strength

The following section reviews the evaluation of joint shear strength according to three different building codes targeted to the assessment of existing structures, i.e., European code [12] (draft of the new generation version), New Zealand code [13] and US code [14]. The background of the analytical method is summarized in the following. A final parametrical comparison is given.

2.2.1. Ec8

The draft of the new Eurocode 8 [12] applies the principal stress criterion for the assessment of an existing RC beam–column joint. With reference to Figure 3a, the joint volume is studied in the plane stress condition. The input forces are the horizontal shear force (assumed to be equal to T) and the axial force in the column (N). The stress condition is studied via Mohr's circle as the one shown in Figure 3b. Both the cases of un-reinforced and reinforced joint are represented.

When the principal tensile stress reaches f_{ct} the joint shear stress (τ_ρ), for a reinforced joint, can be written as follows:

$$\tau_\rho = f_c \sqrt{\left(v \rho_{sh} + \frac{f_{ct}}{f_c}\right) \left(v + \frac{f_{ct}}{f_c}\right)}, \quad (5)$$

where:

- $\rho_{sh} = \frac{A_{sh}}{A_b}$ is the reinforcement ratio;
- $v = \frac{N}{A_c f_c}$ is the normalized axial force.

The shear stress is usually divided by the factor $\sqrt{f_c}$. Such normalization is commonly adopted by US authors and building codes, the cracking resistance of a beam–column joint being assimilated to the tensile strength of concrete which is traditionally given as a function of $\sqrt{f_c}$ [15]. Assuming ρ_{sh} is equal to zero in Equation (5) (un-reinforced joint), the tensile normalized shear strength ($v_{j,t}$) is written as follows:

$$v_{j,t} = \frac{f_{ct}}{\sqrt{f_c}} \sqrt{1 + \frac{v f_c}{f_{ct}}}. \quad (6)$$

The procedure to obtain the compressive normalized shear strength ($v_{j,c}$) is similar to that presented above for $v_{j,t}$. First, Mohr's circle is used to obtain the shear stress by imposing the value ηf_c for the compressive principal stress, where $\eta = 0.55[\min(1; 30/f_c)]^{1/3}$ is a reduction factor which takes into account the detrimental effect of transversal tensile strains. Second, $\sqrt{f_c}$ normalization is used. Finally, the expression is as follows:

$$v_{j,c} = \eta \frac{f_c}{\sqrt{f_c}} \sqrt{1 - \frac{v}{\eta}}. \quad (7)$$

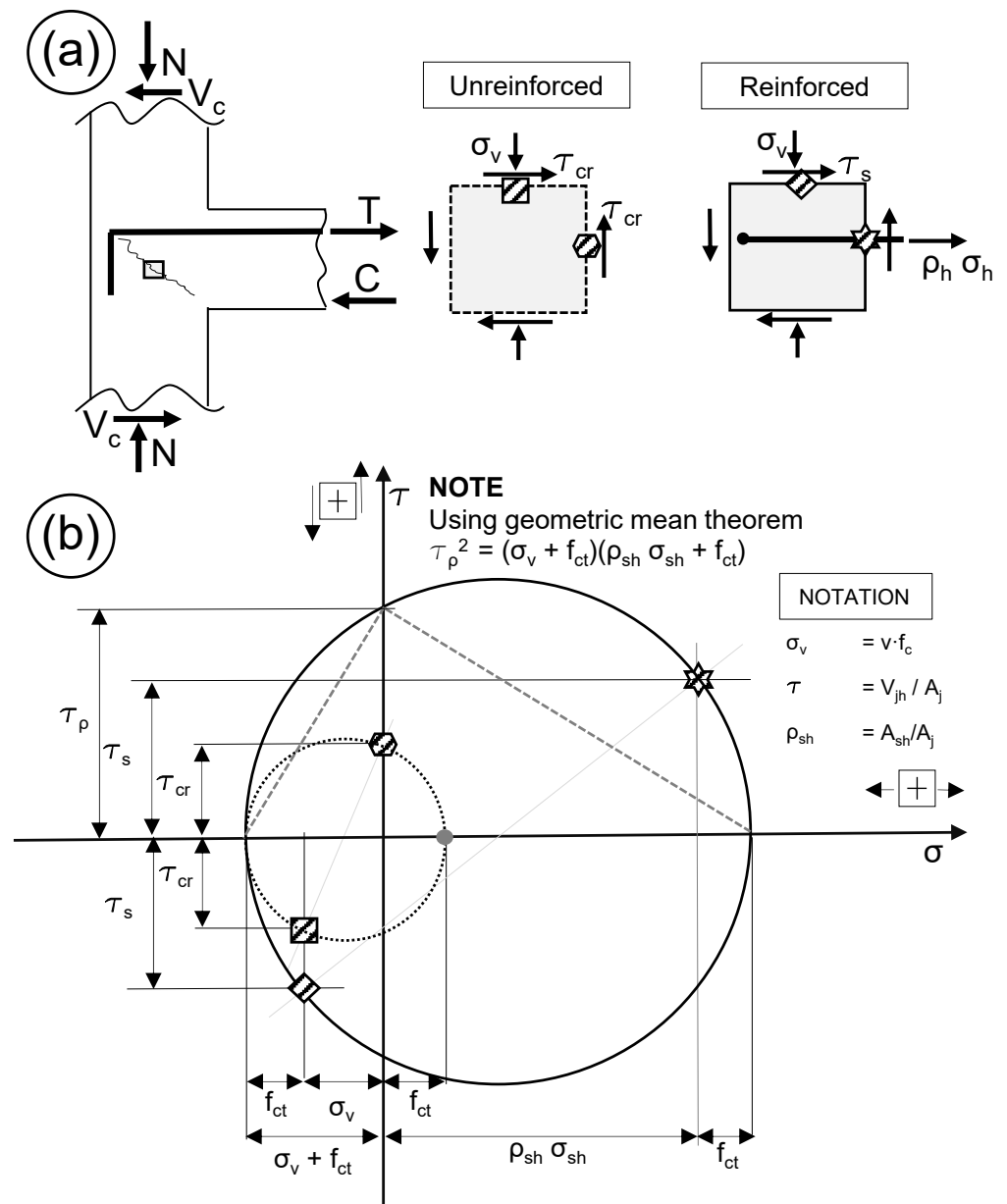


Figure 3. Principal stress method application to beam–column joint: (a) Free body diagram and stress state definition for un-reinforced and reinforced joint; (b) Mohr’s Circle.

2.2.2. Nzsee-2017

Similarly to Eurocode 8, NZSEE-2017 [13] assumes the principal stress method to evaluate the joint shear strength. However, an empirical coefficient (k_j) is used: (i) to define the increased strength of interior joint with respect to exterior; and (ii) to represent the strength reduction at an imposed ductility level. The background of k_j is experimental. Further details are due to Hakuto [16]. k_j values and its effect on the Mohr’s Circle are shown in Figure 4.

The normalized shear strengths, $v_{j,t}$ and $v_{j,c}$, are written as follows:

$$v_{j,t} = \frac{0.85}{\sqrt{f_c}} \sqrt{(k_j \sqrt{f_c})^2 + k_j \sqrt{f_c} v f_c} \tag{8}$$

$$v_{j,c} = \frac{0.85}{\sqrt{f_c}} \sqrt{(0.60 f_c)^2 - 0.60 f_c^2 v}. \tag{9}$$

A reduction of 30% is prescribed for joint shear strength when the joint is subjected to bidirectional loading.

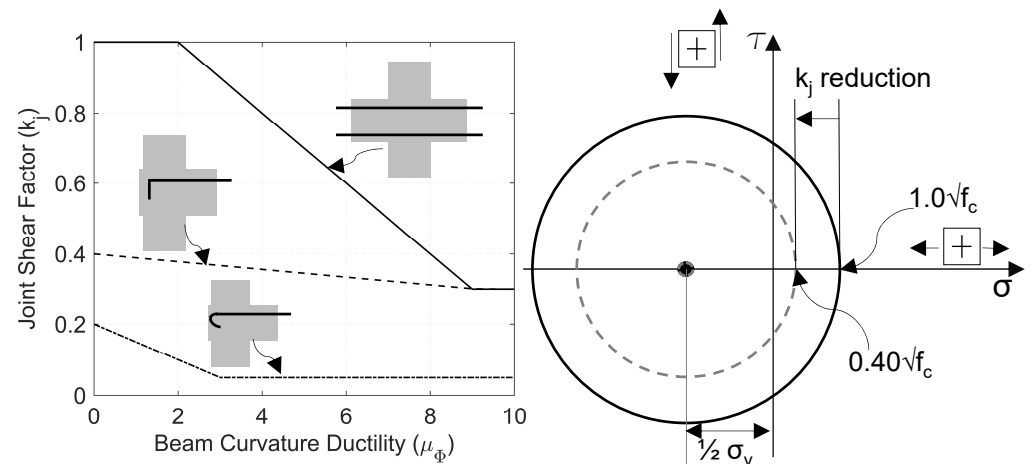


Figure 4. Definition of k_j coefficient according to New Zealand code [13].

2.2.3. Asce41-17

ASCE 41-17 [14] prescribes nominal values for normalized joint shear strength by selecting the joint type (interior or exterior) and the presence of transverse beam (defined as the beam orthogonal to the flexural plane). This definition has been adapted for three-dimensional joints, either having two-ways or three-ways converging beams, by defining the joint type in each flexural plane as shown in Figure 5.

The reduced value of the strength is given for “non-conforming” joints, i.e., joints characterized by the absence of horizontal reinforcement.

Additional provisions for bi-axial strength are given in ACI352 [11], i.e., the elliptical interaction domain is assumed.

2.2.4. Parametrical Comparison

A parametrical analysis was carried out using the predicted values of the normalized shear strength according to the reviewed building codes. The investigated parameters are: (i) the compressive strength of concrete (f_c); and (ii) the normalized axial load (ν) ranging from 10 to 60 MPa and from 0 to 0.70, respectively. The un-reinforced beam–column joints being the target of this paper, Equation (5) was not addressed. A value of k_j equal to 0.40 was assumed for NZSEE2017.

Figure 6a,b represents the EC8 results using Equations (6) and (7), respectively. The condition of ν larger than η implies the lost of meaning for Equation (7), which is then conveniently represented with zero resistance. Figure 6c,d shows the NZSEE2017 outcomes using Equations (8) and (9), respectively. Fixed values of shear strength are given by ASCE41-17 for different joint types, i.e., (INT) interior, (INT-TR) interior with transverse beam, (EXT) exterior, and (EXT-TR) exterior with transverse beam.

As expected, for un-reinforced joints, tensile strength is generally lower with respect to the compressive one. Exceptions are due to large values of the normalized axial force contemporary to low values of f_c , e.g., ν larger than 0.5 and f_c lower than 30 MPa for EC8.

The normalized shear strength calculated according to the reviewed building codes partly illustrates substantial differences to the point that a variation in the safety margin should be expected if an existing structure is assessed according to different codes as will be proved in the following numerical study.

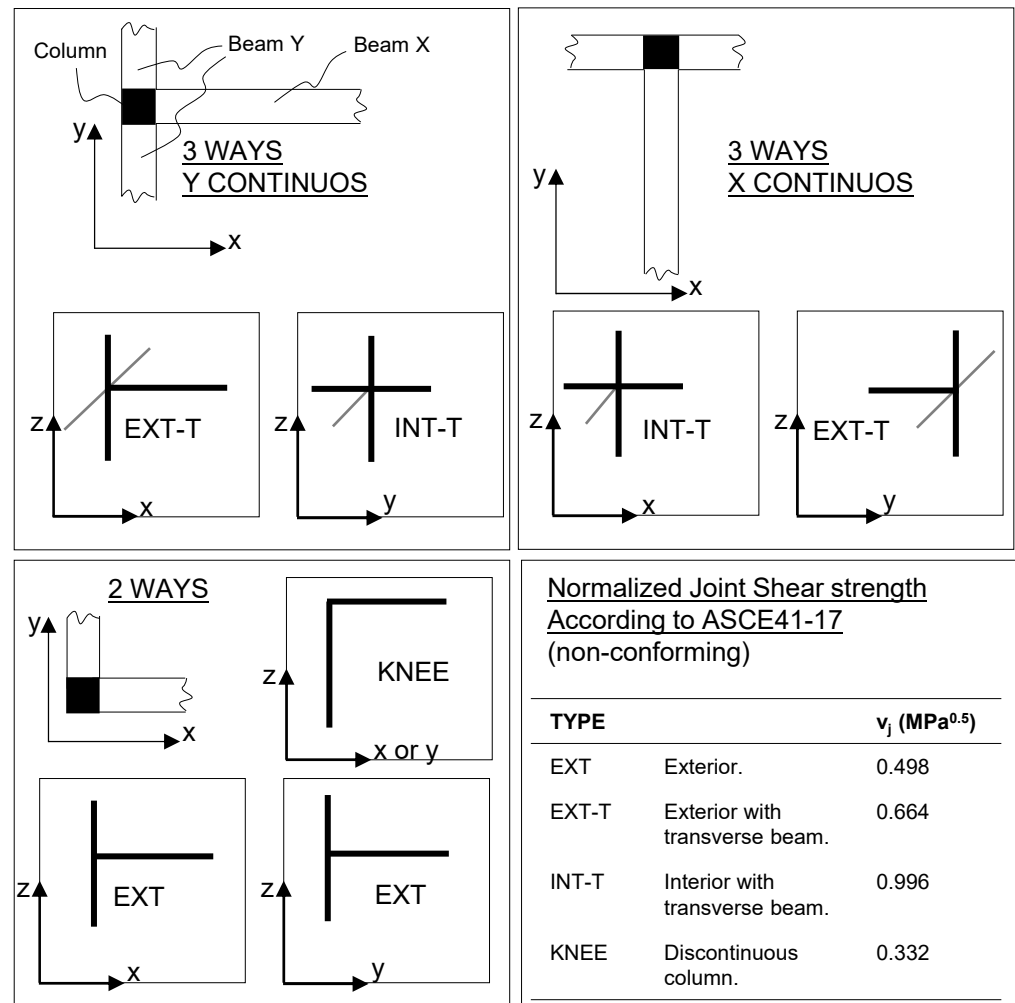


Figure 5. Beam–column classification according to ASCE41-17 [14].

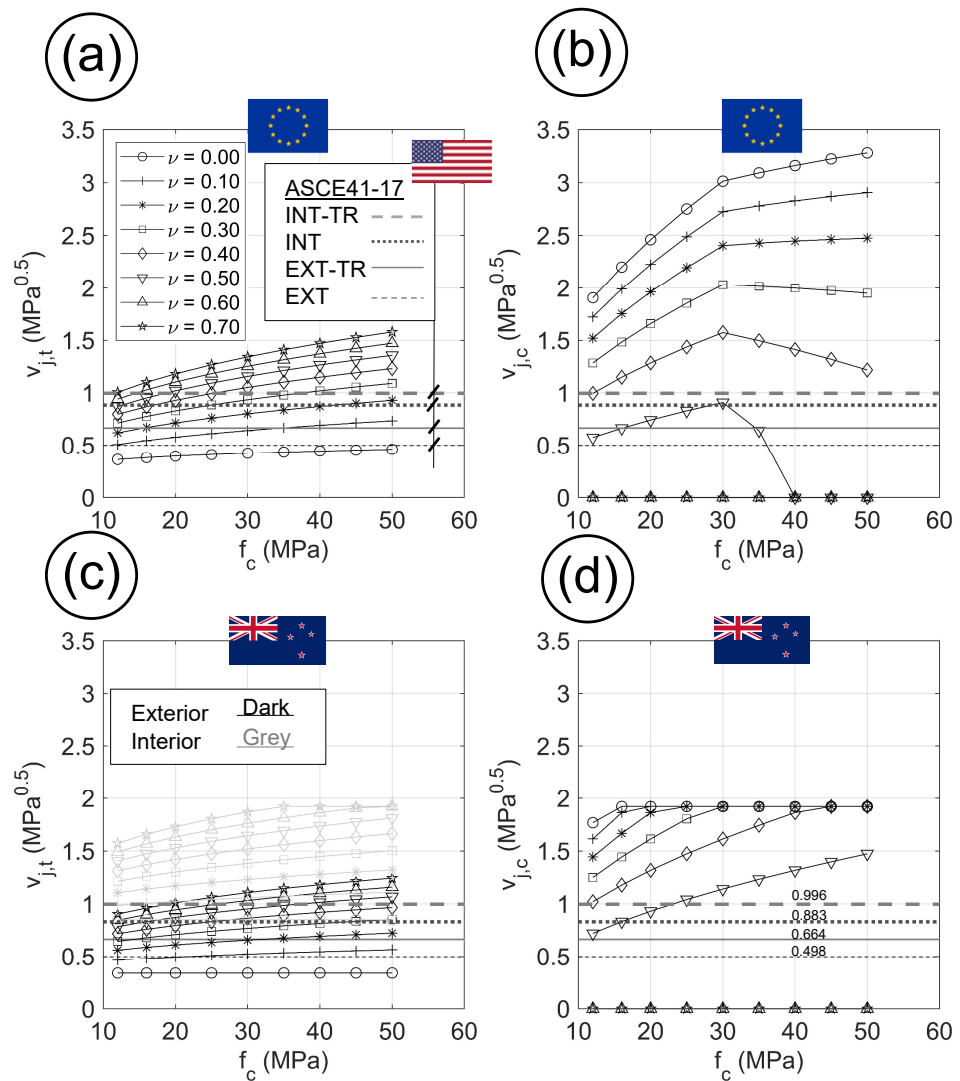


Figure 6. Results for parametrical analysis on beam–column joint strength (normalized shear strength v_j [$\text{MPa}^{0.5}$]) predicted by different building codes: (a) Equation (6); (b) Equation (7); (c) Equation (8); (d) Equation (9). All the plots includes the constant values of the prediction given by ASCE41-17 [14].

3. Numerical Study

3.1. Scope

A numerical study is presented addressing the estimated shear demand for beam–column joints of an RC 3D frame structure using different methods for the seismic structural analysis, such as modal-response-spectrum-analysis (MRSA), non-linear-static-analysis (NLSA) and non-linear-time-history (NLTH). The selected benchmark structure is the SPEAR frame which was tested in 2004 pseudo-dynamically (PsD) at the European Joint Research Centre at Ispra, Italy. Details of the structure as well as of the structural analysis methods are given in the following.

3.2. Details of SPEAR Frame

The frame was a three storey frame with two bays in both plan directions. The details of the structures are represented in Figure 7.

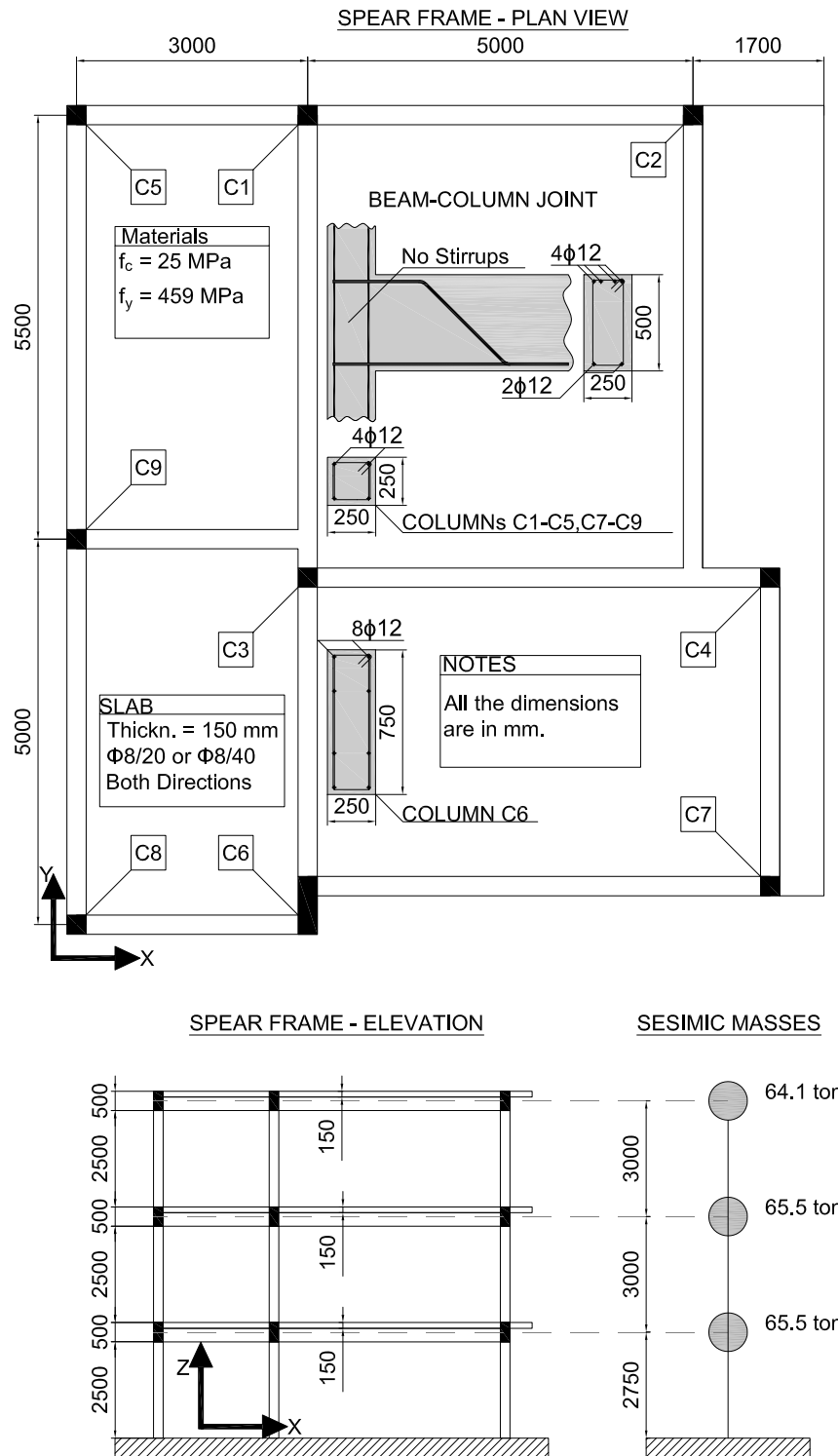


Figure 7. SPEAR frame layout.

The structure was conceived by Prof. Fardis [17] as a typical RC structure designed for gravity load only. Beams had a 250 × 500 mm cross-section, column had 250 × 250 mm cross-section, 250 × 750 mm cross-section was used for one column. Flat slab had 150 mm thickness with reinforcement mesh grid of 8 mm diameter bar spaced at 20 cm or 40 cm. Beam–column joints were characterized by the absence of stirrups and straight anchorage for the beam longitudinal reinforcement both at the bottom (two bars with diameter 12 mm)

and top layers (four bars with diameter 12 mm). The estimated seismic masses were 65.5 tons for the first and second floors and 64.1 for the third floor.

The structure was tested both in the as-built condition and retrofitted using different techniques for column strengthening, i.e., fiber-reinforced polymer (FRP) or jacketing [17,18]. PsD tests were carried out with bi-axial seismic input. Montenegro 1979 Herceg–Novi ground motion record was selected. The recordings of the two orthogonal components of horizontal accelerations were modified from natural records to be compatible with the Eurocode 8 [10], Type 1 design spectrum, soil type C and 5% damping [19]. Time histories were scaled to conventional values of peak-ground-acceleration (PGA) equal to 0.15 g and 0.20 g.

During the strongest test (0.20 g of PGA), the obtained displacements at the third floor were in the order of 100 mm in both directions and 20 mrad of floor rotation. Columns were the most damaged members of the structure, especially at the second story; significant inclined cracks were observed on their compressive sides and on the tensile side at the beam–column interface [20]. The damage on the rectangular column C6 was less important, even though the crushing of concrete and cracks at the interface with beams were observed [18].

Through the years many researchers [7] addressed the SPEAR frame to validate numerical models; a survey of the most relevant studies is summarized in Table 1. NLTH analysis in conjunction with frame modeling was often adopted. In one case [21] brick finite elements were used. The validation chain usually adopted: (i) experimental results of the PsD test against NLTH; and (ii) NLTH against either NLSA or MRSA. To facilitate the validation, the modeling criteria used in this study, which are summarized in the following, were generally compliant with those assumed by the surveyed literature.

Table 1. Literature survey of numerical studies addressing SPEAR frame.

Author	Ele ^(a)	Type of Analysis			Scope of Investigation	Refs.
		MRSA	NLSA	NLTH		
Bento	F	✗	✓	✓	Validation of non-linear static procedures.	[22]
Bhatt	F	✗	✓	✓	Extension of Capacity Spectrum Method [23] to non-symmetric case.	[24]
Brun	F	✗	✗	✓	Validation of GC [25] time integration algorithms.	[26]
Di Ludovico	F	✗	✓	✓	Assessment of experimental results.	[27]
Dolsek	F	✗	✓	✗	Validation of a probabilistic seismic performance assessment.	[28]
Fajfar	F	✓	✗	✓	Definition of torsional amplification to be applied to N2 method [29].	[30,31]
Kosmopoulos	F	✓	✗	✓	Validation of chord rotation demand from MRSA.	[17]
Mola	F	✗	✓	✓	Assessment of experimental results.	[32]
Pardalopoulos	F	✗	✗	✓	Validation of lumped non-linear hinges representing brittle failures.	[33]
Reynouard	B	✗	✗	✓	Assessment of experimental results.	[21]
Rozman	F	✓	✓	✗	Comparison of seismic conforming variants of SPEAR frame.	[34]
Stratan	F	✗	✓	✓	Assessment of experimental results. Influence of modelling assumptions.	[35,36]

Notes. ^(a) Type of elements: [F] frame; [B] Bricks or shells.

3.3. Structural Modeling and Seismic Demand

A three dimensional frame structural model was developed using SAP2000 [37]. Details are given in Figure 8. Beams and columns were modeled using a lumped-plasticity [38] approach. Specifically, elastic 3D frame elements (two nodes, 12 dofs) were used in conjunction with rotational non-linear springs (plastic hinges) assigned at the same location (zero

length) of the extreme nodes. The element size was kept equal to one half of the inter-storey height for the columns and half-bay for the beams. Columns were clamped at the base. Floor masses were lumped at the centers of mass. Diaphragm kinematic constraint was assigned at each floor.

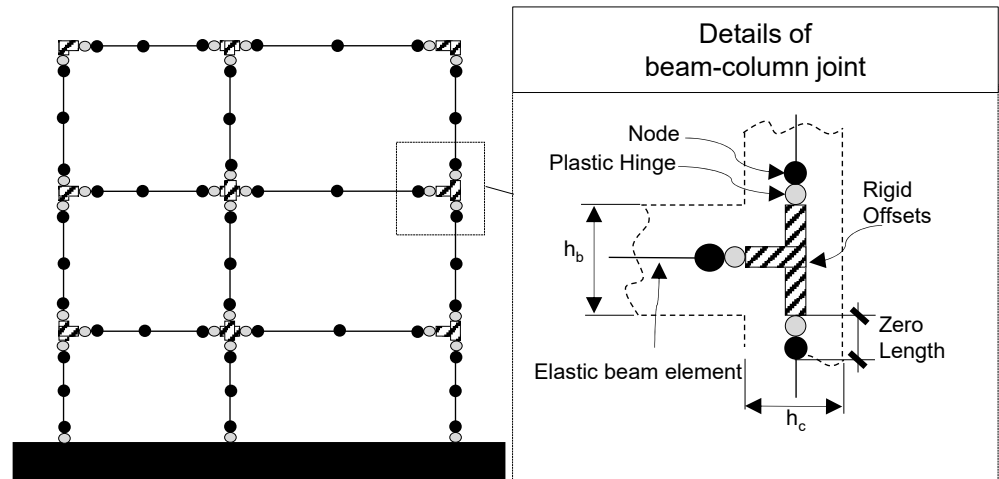


Figure 8. Modeling features.

The plastic hinges’ constitutive law (moment vs rotation) was defined for each beam and columns, considering different axial load levels for the latter. In particular, a preliminary sectional analysis was carried out using Response2000 [39]. The yielding moment was evaluated from the moment–curvature diagrams (examples are given in Figure 9). Plastic rotation capacities were attributed empirically as shown in Figure 10, complying with the FEMA356 [40], similarly with what was presented by Stratan [35]. Takeda [41] model was used for the hysteretic response.

Slab contribution to the flexural capacity of the beam was neglected because it would activate only for large ductility demand [42], which was not reached at the imposed seismic level. Furthermore, a weak column condition is recognized even using the beam’s nominal dimensions, as can be inferred from Figure 9. Indeed, despite the case of the strong column (cross-section 25 × 75 cm), beam bending capacity (nominal cross section 25 × 50 cm) results in being larger with respect to the columns having a 25 × 25 cm cross-section.

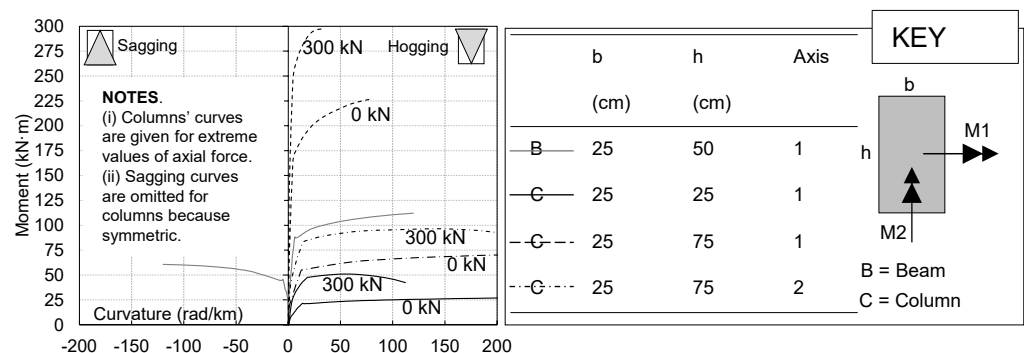


Figure 9. Moment–curvature diagrams for the cross sections of beams and columns of SPEAR frame. Results were obtained using the software Response 2000 [39].

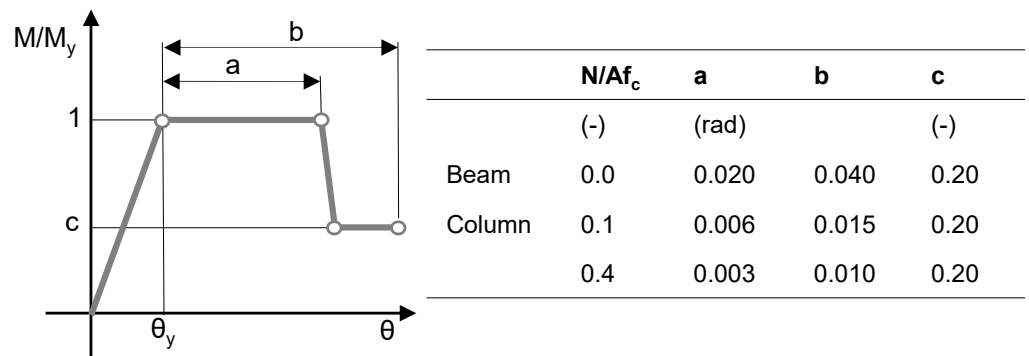


Figure 10. Definition of plastic hinges according to FEMA356 [40].

Beam–column joints were modeled as rigid. The half depth of both the column and beam was set as a rigid length. A discussion about differences in adopting center-line modeling, which assumes beams and columns that are entirely flexible, can be generally found in [43]. Moreover, Stratan [35] studied the influence for SPEAR frame’s joint. In essence, higher shear demand is a consequence of rigid offsets. Center-line modeling may be used as a simple way to account for both the reduction of stiffness and strength due to additional deformation in the joint regions [44].

Different methods were used to carry out the seismic structural analysis as presented in Table 2. The seismic demand was chosen such that the comparison between different methods can be sustained as explained in the following.

NLTH assumed Herceg–Novi (1979) spectrum-compatible accelerograms as shown in Figure 11. The original time recordings, available at <http://ngawest2.berkeley.edu> in April 2022, were processed (using OpenSeismoMath [45]) to fit the elastic spectra (5% damping, Type I, Soil C), defined according to Eurocode 8 [10]. This procedure is consistent with what was described by Negro [19] for the execution of the PsD test.

MRSA used a design spectrum. A behavior factor (q) equal to 3.45 was assumed to be similar to that declared by Rozman [34].

NLSA simply assumed 100 mm roof displacement (center of mass), in both x and y directions, as a target displacement. This condition is comparable to the results obtained via both NLTH and MRSA. Gravity load and $P-\Delta$ effect were not taken into account.

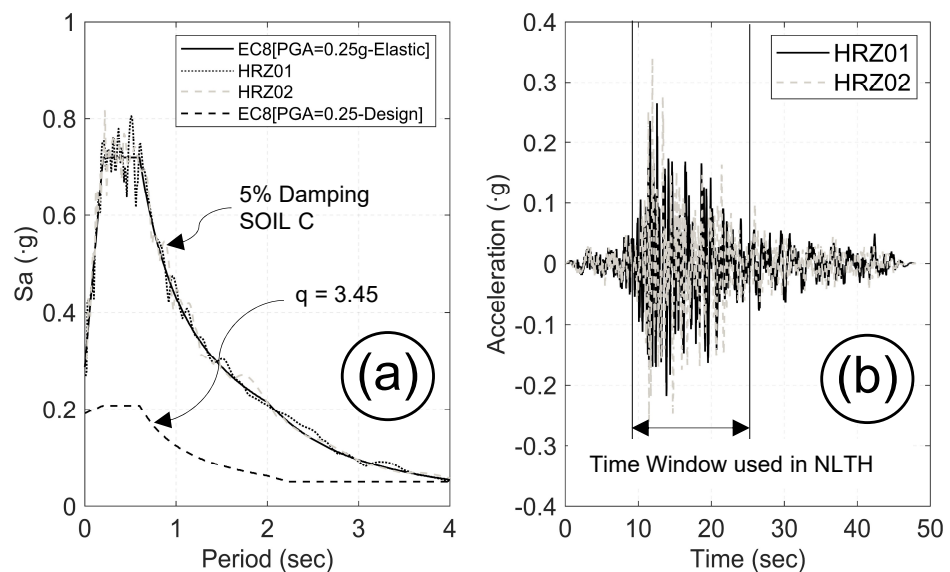


Figure 11. Seismic demand: (a) Response spectrum; (b) Herceg–Novi (1979) acceleration time histories.

Table 2. Details for structural analyses.

Method	Seismic Demand	Notes	Ref. ^(a)	Bi-Dir. ^(b)
MRSA	Design Response Spectrum with $q = 3.45$ according to Figure 11.	Modal Combination uses CQC rule.	[34]	30% rule.
NLSA	Capacity Spectrum with 100 mm target displacement in both directions.	Multi-Modal according to [46].	[18,36]	SRSS.
NLTH	Herceg-Novi Accelerogram (PGA = 0.25 g) according to Figure 11	Direct integration according to [47].	[33]	Simultaneous inputs.

Notes. ^(a) References used to compare the numerical results. ^(b) Method used to account for bi-directional seismic demand.

3.4. Validation

The structural analyses were validated against both experimental and numerical results derived from the literature. Results are briefly discussed, in the following, assuming the global behavior of the structure as a target, e.g., inter-story drifts, capacity curves, displacement time histories.

The influence of beam–column joints modeling was recognized by modal analysis. In particular, rigid offsets gave shorter periods for the first three modes as can be inferred from Table 3. Furthermore, the first three modes (Figure 12a) amount to almost 80% of the participating mass in both x and y directions. Clearly, the third mode involved torsional behavior, although only partly confirmed by previous numerical investigation. Nevertheless, MRSA produced comparable results with respect to Rozman [34] for drift values as shown in Figure 12b.

Table 3. Validation of Modal Analysis results.

Author/Model	Ref.	T_1 (s)	M_X (%)	M_Y (%)	T_2 (s)	M_X (%)	M_Y (%)	T_3 (s)	M_X (%)	M_Y (%)
DiLudovico	[27]	0.62	71.80	5.80	0.54	12.40	60.50	0.43	12.40	60.50
Reynouard	[21]	0.64	-	-	0.54	-	-	0.42	-	-
Stratan	[36]	0.57	-	-	0.48	-	-	0.39	-	-
Rozman	[34]	0.80	69.00	4.80	0.69	15.60	47.80	0.58	2.70	30.30
Negro (Experimental)	[19]	0.84	-	-	0.78	-	-	0.67	-	-
RIGID	This paper	0.85	55.00	0.00	0.47	2.18	56.00	0.35	31.00	27.00
FLEXI	This paper	1.24	54.00	0.00	0.64	2.10	56.00	0.50	31.00	27.00

Notes. M_X and M_Y are the participating masses in X and Y direction, respectively.

Results of NLSA are shown in Figure 13. For the sake of validation, two different load patterns were adopted, i.e., uniform distribution of forces and modal; the latter resulting in reduced lateral load bearing capacity. Plastic hinges formed in the columns. Most of the beams remained in the elastic regime. This evidence agreed with what was presented by Rozman [34].

Figure 14 shows the resulting displacement history (roof) in the y direction obtained via NLTH. The comparison with experimental outcomes shows that agreement was found for the oscillation period, the differences in peak values being in line with those obtained, for instance, by Pardalopoulos [33].

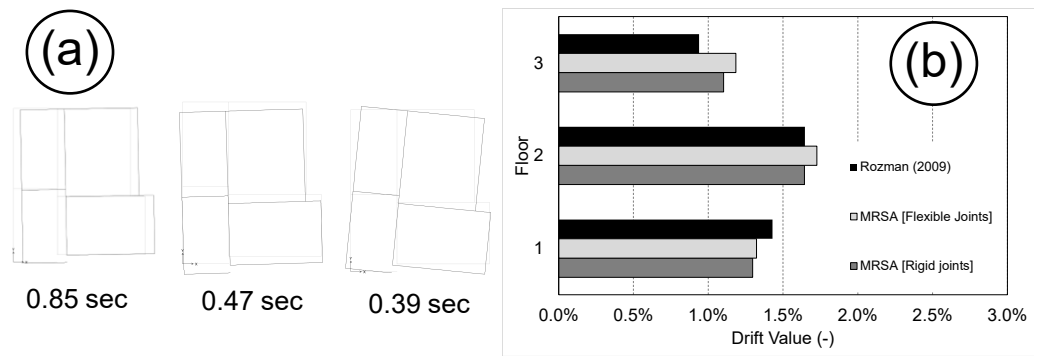


Figure 12. Validation of MRSA applied to the SPEAR frame: (a) Modal analysis results [Note. The first three relevant modes amount 86% and 82% of participating masses in X and Y directions, respectively]; (b) MRSA drifts results.

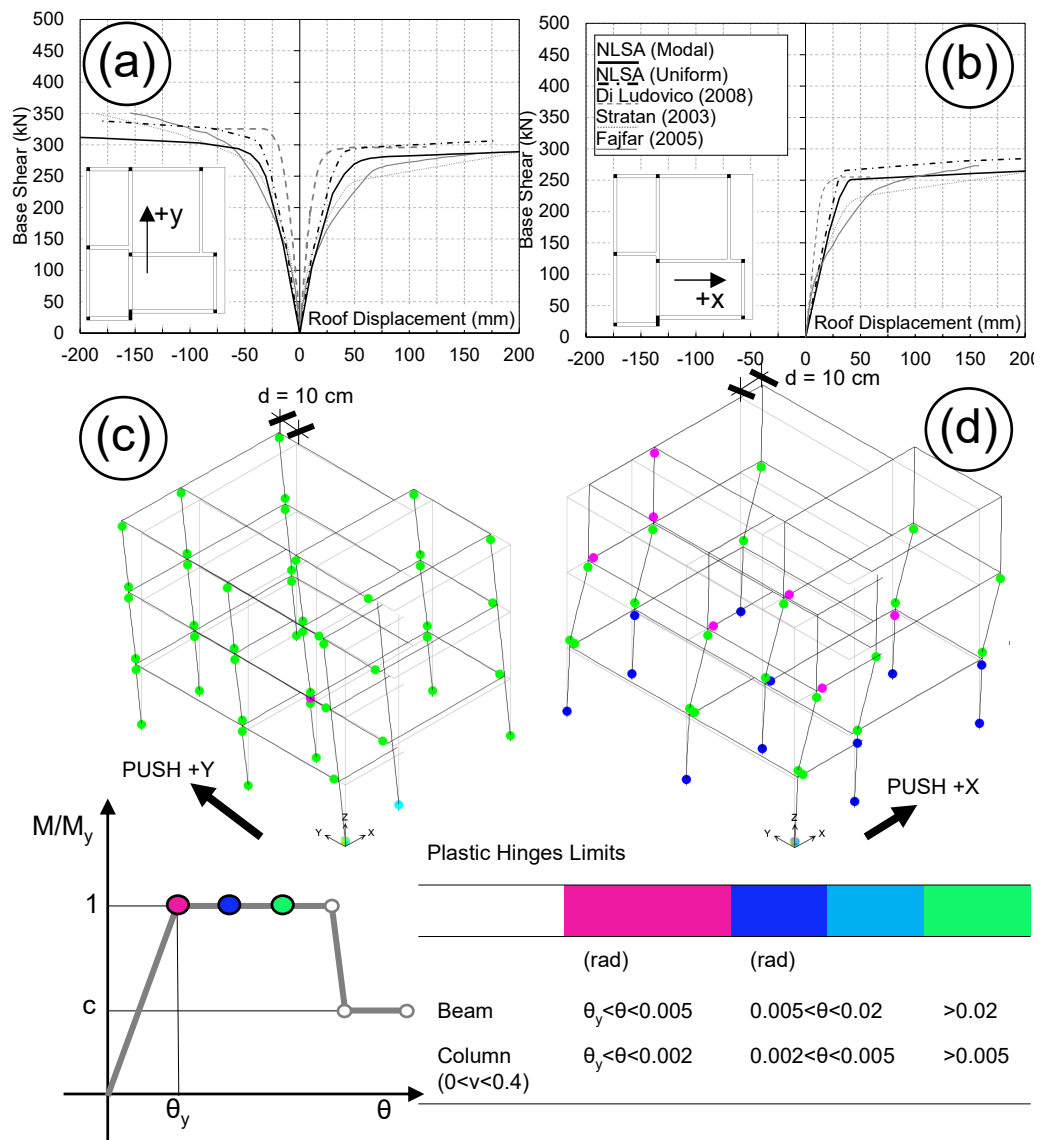


Figure 13. Validation of NLSA applied to the SPEAR frame: (a,b) capacity curves in y and x directions, respectively; (c,d) plastic hinges rotation at 10 cm roof displacement in y and x-directions, respectively. The Reader is referred to the color version of this figure.

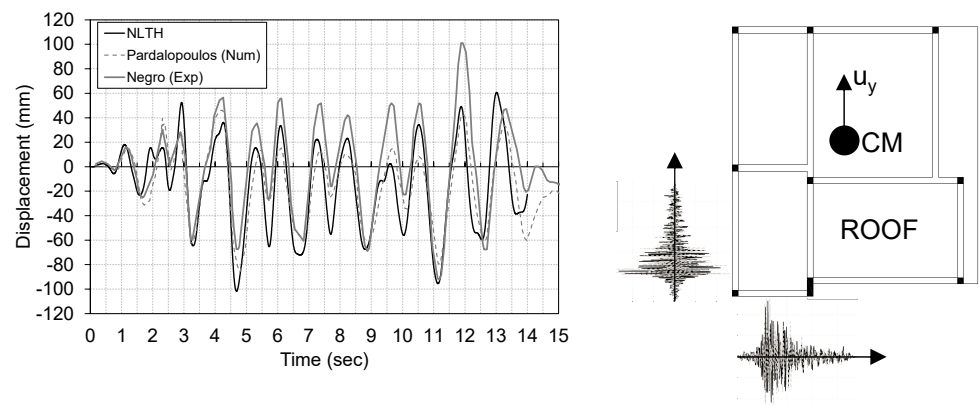


Figure 14. Validation of NLTH applied to the SPEAR frame, y-displacement at the roof.

4. Results and Discussion

4.1. Shear Demand at a Joint

The shear demand at a beam–column joint is not conventionally given as an output by commercial FEM software, thus post-processing is needed. Figure 15 shows the key aspects of the implemented post-processing. At the joint labeled “i” each converging beam delivers a bending moment, represented as arrows in the x-y plane. The horizontal shear demand (V_{jhx} and V_{jhy}) is given in each flexural plane as the summation of T -forces contribution coming from left and right side of the column neglecting the column’s shear. The T forces represent the resultant of stresses at the column–face cross section under the applied bending moment. For the sake of simplicity, a fixed value of the internal lever arm is assumed equal to 0.83 times the effective depth of the beam. Different assumptions should not lead to significant changes for the final shear demand [48].

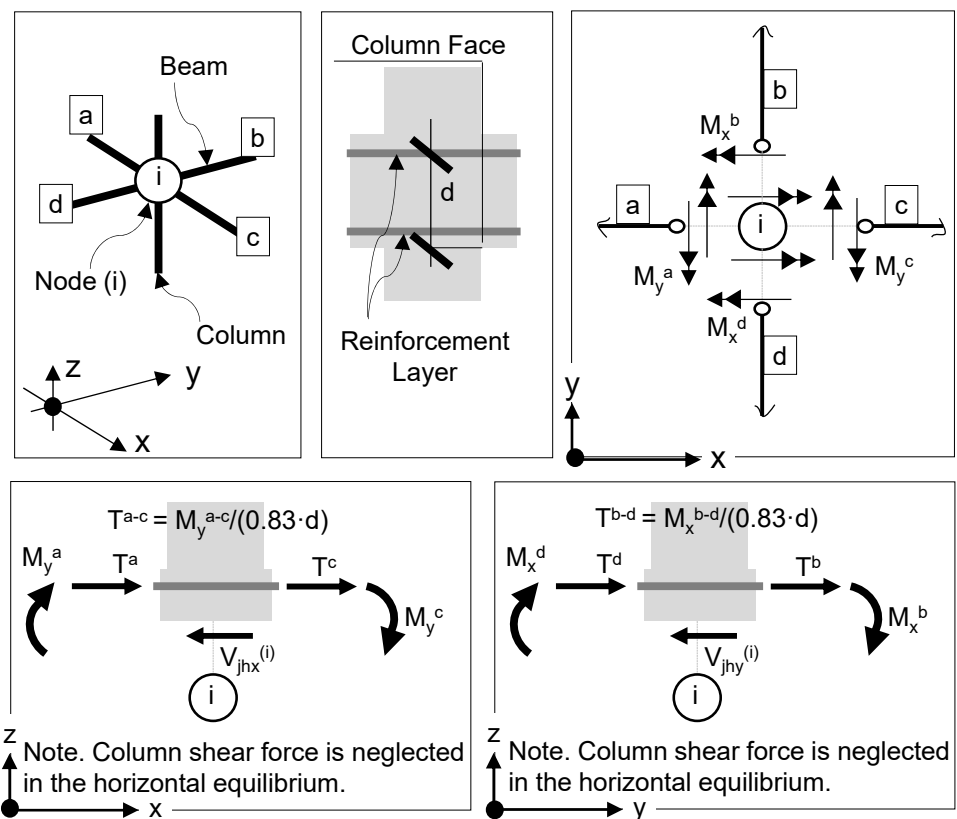


Figure 15. Post-process procedure to evaluate shear demand at beam–column joint “i”. (Note “a”, “b”, “c”, “d” labels define the converging beams at the node).

Considering a practical assessment scenario, the designer might be interested in envelope values. In this regard, the following additional assumptions either on modal combination or bi-directional seismic demand were made for the different analysis methods:

- (MRSa) Maximum values of shear demand at a joint are evaluated, considering the 30% rule for the bi-directional combination. Modal contributions were summed using the complete-quadratic combination (CQC);
- (NLSa) Pushover curves were calculated using the modal force distribution for the first three modes. Specifically, target displacements were assumed in the x-direction for the mode “1” and in the y-direction for the mode “2”. Mode “3” being torsional, both the $\pm x$ and $\pm y$ directions of target displacements were considered. Subsequently, idealization of the pushover curve into a bi-linear curve is made. Shear demand at a joint is extracted for each idealized pushover curve, at the target displacement. The final shear demand is then computed, summing the modal contribution using CQC. This procedure is compliant with what was proposed by Chopra [46], named modal-pushover-analysis (MPA);
- (NLTH) Extreme values of shear demand at a joint are extracted from time histories. Acceleration of time histories apply simultaneously in $\pm x$ and $\pm y$ directions. Envelope of the results coming from different direction signs is made.

To summarize, the shear demand at each flexural plane of a beam–column joint is computed as a post-process starting from values of beams’ bending moments converging at one node. Two major hypotheses were made: (i) the internal lever arm at the column face cross section of the beam is assumed to be constant; and (ii) the contribution to the horizontal equilibrium of the column’s shear is neglected. The latter assumption has already been discussed in Section 2.1, defining the joint shear demand for a planar joint.

Different strategies with respect to the one proposed in this study might facilitate the output of shear demand. Usually they imply additional dofs for the numerical model. As an example, explicit joint modeling can be pursued via single or multi-springs [5]. Besides, the introduction of a stiff “shear hinge” was recently proposed by Pardalopoulos [33]. It is worth mentioning, though, that the introduction of a large stiffness, compared with the flexural stiffness of the beam, remains dubious in the light of numerical errors (the reader is referred to paragraph 8.2.5 of [49]).

4.2. Bi-Axial Shear Demand Using NLTH

Figure 16 shows the bi-axial shear demand curves obtained via NLTH analysis for the case of +x and +y excitation. This condition is privileged in this discussion because it is equal to the pseudo-dynamic experimental input [19]. Additionally, the elliptical domain prescribed by ACI352 [11] is defined at each beam–column joint. The ellipse radii represent the joint shear strength evaluated according to ASCE41-17 [14]. Moreover, the results are compared with the yielding threshold defined according to Equation (4). For the sake of synthesis, only the first and the second floor results are discussed. The latter was characterized by the highest shear demand peaks. The third floor has been omitted because shear demand results were moderate.

As expected, the shear demand does not overcome the yielding threshold, this being inherently included in the definition backbone curves for the beams’ plastic hinges. The elliptical envelope shape of the shear demand orbits is recognized for the majority of the cases. The principal axes of the envelope do not necessarily coincide with x and y directions. This result is consistent with what was proven, numerically, by Menun [50] for bi-axial bending interaction at the columns.

Cases where the shear demand exceeds the shear resistance deserve a particular explanation. In fact, the studies describing the experimental results [18,20] of the SPEAR frame did not report beam–column joint failure and diagonal cracking has been described as occasional. In this regard, and by observing that the shear resistance is exceeded especially for the cases where bi-axial interaction becomes significant (i.e., corner joint), it follows that the elliptical strength domain is conservative. Nothing can be said about a

possible over-estimation of shear demand which cannot be sustained conclusively due to the impossibility to validate the obtained results against experimental references. To the authors' knowledge, only Stratan [36] attempted to numerically evaluate the shear demand at the beam–column joint of the SPEAR frame. Results were reported as mean extreme values of NLTH analysis (the reader may find the definition of mean extreme value in the Section titled “Probability Distribution for extreme values” in [51]). Comparison with those is given in the following. Besides, Pardalopoulos [33] modeled the SPEAR frame including “shear hinges” at beam–column joints but shear demands were not presented explicitly.

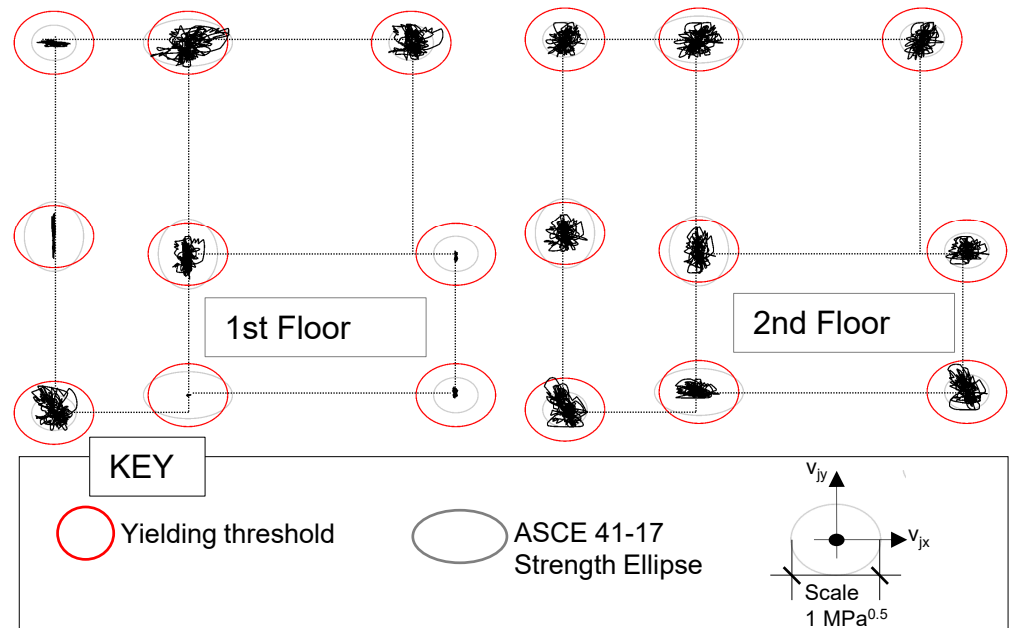


Figure 16. Bi-axial shear demand of beam–column joint obtained with NLTH (Case of +x and +y excitation). The reader is referred to the color version of this figure.

4.3. Evaluated Shear Strength

Shear strengths evaluated according to building codes reviewed in Section 2.2 are graphically presented in Figure 17. The numerical values are given in Table 4. For the sake of synthesis, both the Figure and the Table include also the shear demand which is discussed subsequently.

Shear strength has been evaluated considering the beam–column joints as being three dimensional without stirrups. The definition of joint type, at each flexural plane, according to Figure 5 applies only for ASCE41-17 and NZSEE2017. No distinction is given for EC8. A reduction of 30% has been applied to the strength values of NZSEE2017, complying with the provision for the bi-axial condition. The axial load for the column is considered at the seismic combination. Only tensile failure (e.g., Equation (6)) is reported because it has been recognized as dominant with respect to the compressive. Moreover, a constant value of 0.4 for the coefficient k_j (defined at Figure 4) in Equation (8) has been assumed according to the evidence of reduced ductility demand for the beam.

Differences between predicted values of shear strength, using different building codes, are recognized. NZSE2017 gives generally the lowest prediction with respect to EC8 and ASCE41-17. The latter prevails for knee joints. Figure 18 shows the ratio between the evaluated shear demand via NLTH (assumed as the most accurate with respect to NLSA and MRSA) with respect to predicted shear strength (demand-to-strength) as a function of the different joint type. Demand-to-strength ratio is expected to be less than one according to the experimental absence of joint shear failure. Values larger than one are recognized mostly for exterior joint type. This condition can be explained as an excess of safety margins for corner joints if the plane exterior joint type is attributed to both the flexural planes.

Probably, a larger strength should be expected as the result of the confinement offered by the beams in both directions as claimed by Kurose [52] discussing experimental evidence.

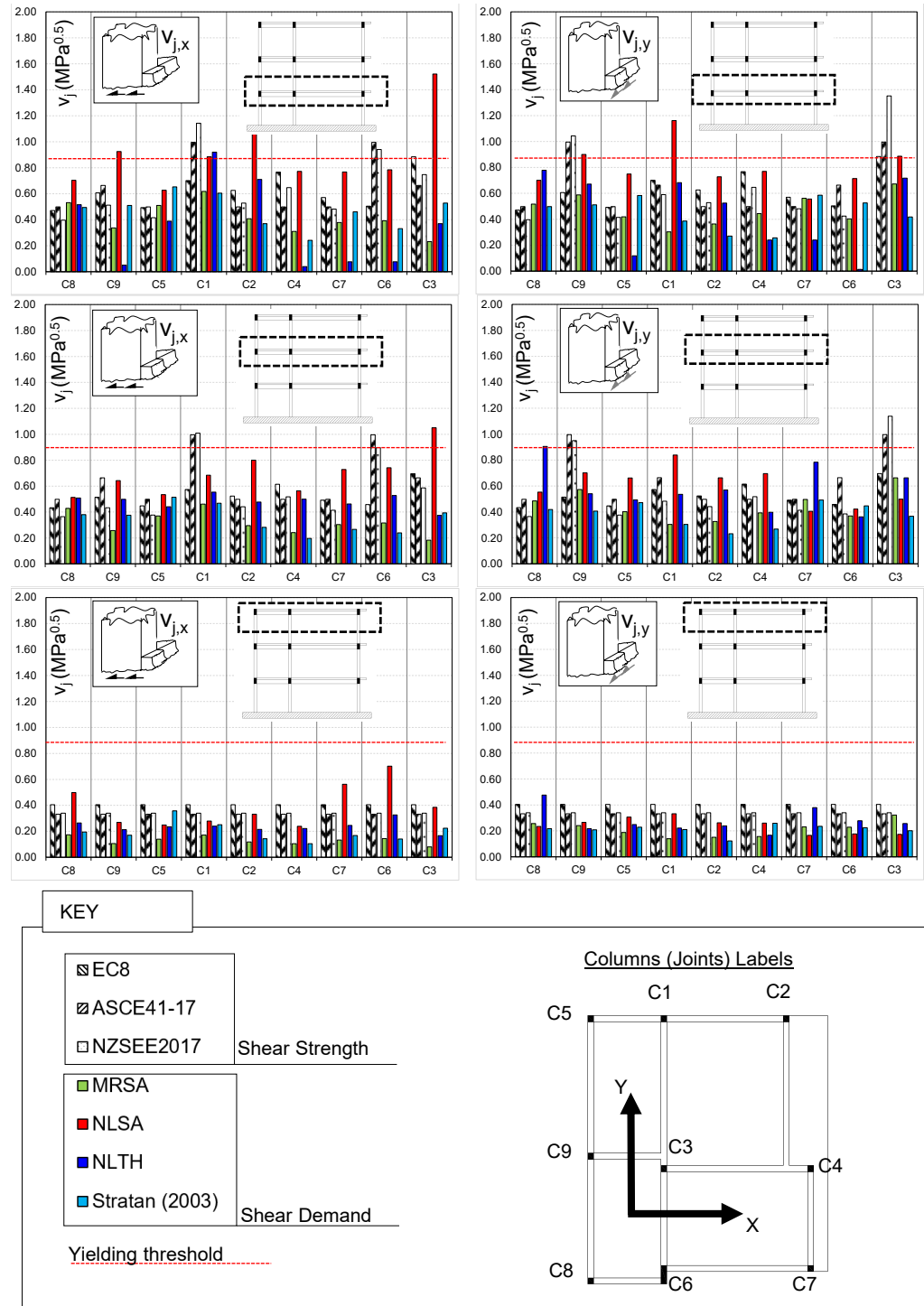


Figure 17. Evaluated joint shear demand and strength for beam–column joints of SPEAR frame. The reader is referred to the color version of this figure.

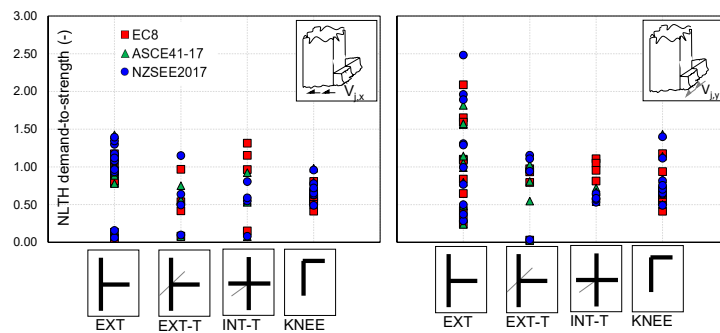


Figure 18. NLTH Demand-to-strength ratios for the beam–column joints of SPEAR frame. The reader is referred to the color version of this figure. (Note. NLTH demands are evaluated using extreme absolute values.)

Table 4. Shear strength and demand evaluated for beam–column joints of the SPEAR frame.

COL	FL	T-XZ	T-YZ	ν	Shear Strength			Shear Demand							
					$\min(v_{j,x})$	$\min(v_{j,y})$	$\min(v_{j,z})$	$\max(v_{j,x})$	$\max(v_{j,y})$	$\max(v_{j,z})$	$\max(v_{j,y})$				
(a)	(b)	(c)	(d)	(e)	<i>All the Values Are Expressed in MPa^{0.5}</i>										
					EC8	ASCE41-17	NZSEE2017	MRSA	NLSA	NLTH					
					$v_{j,x-y}$	$v_{j,x}$	$v_{j,y}$	$v_{j,x}$	$v_{j,y}$	$v_{j,x}$	$v_{j,y}$	$v_{j,x}$	$v_{j,y}$	$v_{j,x}$	$v_{j,y}$
C8	1	EXT	EXT	0.03	0.471	0.498	0.498	0.397	0.397	0.531	0.517	0.703	0.700	0.515	0.778
C9	1	EXT-T	INT-T	0.10	0.607	0.664	0.996	0.511	1.043	0.337	0.588	0.925	0.900	0.049	0.672
C5	1	EXT	EXT	0.04	0.493	0.498	0.498	0.415	0.415	0.509	0.419	0.627	0.750	0.388	0.119
C1	1	INT-T	EXT-T	0.16	0.701	0.996	0.664	1.143	0.591	0.618	0.303	0.884	1.161	0.920	0.683
C2	1	EXT	EXT	0.11	0.626	0.498	0.498	0.528	0.528	0.408	0.364	1.074	0.728	0.709	0.525
C4	1	EXT	EXT	0.21	0.767	0.498	0.498	0.647	0.647	0.309	0.444	0.771	0.769	0.039	0.241
C7	1	EXT	EXT	0.08	0.571	0.498	0.498	0.481	0.481	0.378	0.562	0.768	0.556	0.075	0.241
C6	1	INT-T	EXT-T	0.04	0.504	0.996	0.664	0.940	0.425	0.391	0.404	0.784	0.714	0.075	0.014
C3	1	EXT-T	INT-T	0.31	0.884	0.664	0.996	0.747	1.352	0.231	0.673	1.521	0.886	0.369	0.718
C8	2	EXT	EXT	0.01	0.433	0.498	0.498	0.364	0.364	0.429	0.486	0.512	0.553	0.508	0.905
C9	2	EXT-T	INT-T	0.05	0.514	0.664	0.996	0.433	0.950	0.257	0.573	0.642	0.701	0.498	0.540
C5	2	EXT	EXT	0.02	0.447	0.498	0.498	0.377	0.377	0.370	0.402	0.535	0.662	0.441	0.493
C1	2	INT-T	EXT-T	0.08	0.574	0.996	0.664	1.009	0.484	0.462	0.304	0.684	0.838	0.553	0.536
C2	2	EXT	EXT	0.05	0.524	0.498	0.498	0.441	0.441	0.296	0.327	0.800	0.664	0.477	0.569
C4	2	EXT	EXT	0.11	0.614	0.498	0.498	0.518	0.518	0.241	0.393	0.563	0.695	0.500	0.397
C7	2	EXT	EXT	0.04	0.491	0.498	0.498	0.414	0.414	0.304	0.497	0.728	0.406	0.463	0.783
C6	2	INT-T	EXT-T	0.02	0.458	0.996	0.664	0.897	0.385	0.315	0.369	0.741	0.422	0.528	0.363
C3	2	EXT-T	INT-T	0.16	0.695	0.664	0.996	0.587	1.138	0.183	0.663	1.050	0.499	0.374	0.664
C8	3	KNEE	KNEE	0.00	0.404	0.332	0.332	0.340	0.340	0.173	0.257	0.498	0.234	0.195	0.217
C9	3	KNEE	KNEE	0.00	0.404	0.332	0.332	0.340	0.340	0.106	0.241	0.268	0.265	0.170	0.208
C5	3	KNEE	KNEE	0.00	0.404	0.332	0.332	0.340	0.340	0.140	0.188	0.249	0.306	0.358	0.228
C1	3	KNEE	KNEE	0.00	0.404	0.332	0.332	0.340	0.340	0.170	0.140	0.279	0.332	0.250	0.210
C2	3	KNEE	KNEE	0.00	0.404	0.332	0.332	0.340	0.340	0.118	0.151	0.332	0.263	0.143	0.123
C4	3	KNEE	KNEE	0.00	0.404	0.332	0.332	0.340	0.340	0.104	0.156	0.239	0.260	0.105	0.259
C7	3	KNEE	KNEE	0.00	0.404	0.332	0.332	0.340	0.340	0.133	0.230	0.562	0.166	0.168	0.235
C6	3	KNEE	KNEE	0.00	0.404	0.332	0.332	0.340	0.340	0.144	0.229	0.702	0.177	0.141	0.224
C3	3	KNEE	KNEE	0.00	0.404	0.332	0.332	0.340	0.340	0.080	0.323	0.384	0.174	0.224	0.201

Notes. (a) Column label according to Figure 7. (b) Floor number. (c,d) Joint type according to Figure 5. (e) Normalized axial load at top portion of the column. Shear demand at yielding of beam’s longitudinal reinforcement (top layer) is equal to 0.89 MPa^{0.5}.

To summarize, beam–column joints of the SPEAR frame showed significant strength differences. Two major aspects impacted the most, i.e.: (i) the definition of the joint type in each flexural plane; and (ii) the use of a different building code. For the latter, a discussion on the strength accuracy (e.g., [4]) cannot be sustained conclusively because the compared shear demands represent a condition far from failure, as it was observed experimentally.

4.4. Comparison of Shear Demands

The envelope values of shear demand, computed for different structural analysis methods, are reported in Table 4 and Figure 17.

It is clearly recognized that NLSA: (i) gave larger values if compared with MRSA and NLTH; and (ii) generally exceeded the lowest predicted strength. The latter, which contradicts the experimental evidence, can be partly sustained by recalling what was claimed by Chopra for the estimation of plastic hinge rotations using the modal-pushover (MPA) [53]: *...All pushover analysis procedures considered do not seem to compute accurately local response quantities, such as hinge plastic rotations. Thus, the structural engineering profession should examine the present trend of comparing computed hinge plastic rotations against rotation limits established in FEMA-273 to judge structural performance. Perhaps structural performance evaluation should be based on storey drifts that are known to be closely related to damage and can be estimated to a higher degree of accuracy by pushover analyses.* In this context, element forces could also be assimilated to local response quantities, thus less accuracy should be expected when MPA is employed. As a proof of that, cases where the estimated shear demand overcame the yielding force were recognized. Specifically, according to Equation (4), a value of $0.88 \text{ MPa}^{0.5}$ was obtained for the hogging type moment, having considered an overstrength factor equal to $\gamma_{Rd} 1.25$. Although the sagging type moment gave half of the value, the comparison with envelopes of shear demand can be sustained only for the former case.

While the adoption of MPA has been considered as the state-of-the art for the inelastic analysis of non-symmetric structure (possibly torsionally flexible) under bi-axial seismic input, the authors are aware of other procedures such as the “modified” N2 method [30,31]. Although its computational effort is reduced with respect to MPA, the same lack of accuracy in predicting the element forces should be expected.

Differences were recognized by comparing NLTH values with those given by Stratan [36]. The deviation trend is not easily discernible to the point that, aside from general differences in modeling, both (i) a different definition of shear demand and (ii) use of mean extreme values rather than absolute might have an influence.

Finally, the shear demands are represented as a function joint type in Figure 19. The exterior joints with a transverse beam were characterized by the highest shear demand by using NLSA. Interior joints prevailed with MRSA. NLTH did not show a quite clear trend.

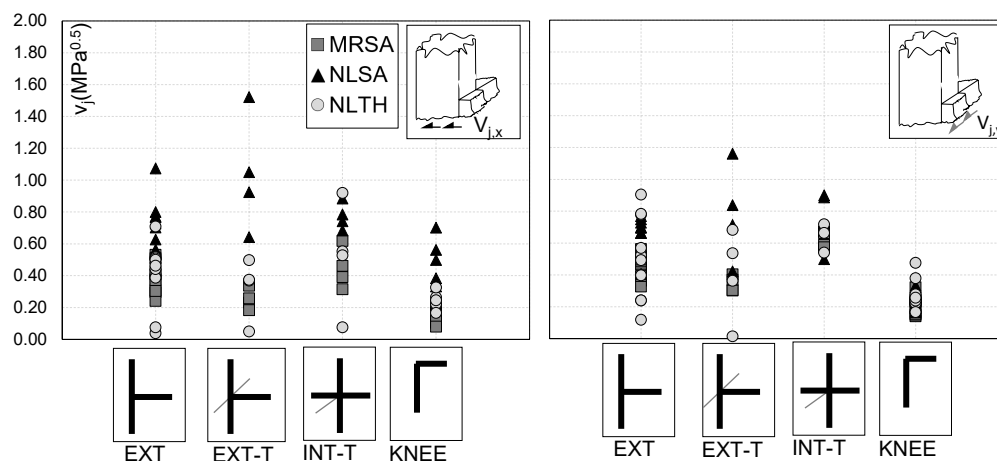


Figure 19. Shear demand of beam–column joints of SPEAR frame as a function of the joint type.

5. Conclusions

A numerical study was presented considering a notorious benchmark in the context of RC structures against earthquake loading, i.e., the SPEAR frame. This paper focused on shear demand at beam–column joints. Results were obtained using a three-dimensional numerical model validated against past studies addressing the same structure. Beam–column joints were modeled with rigid offsets. Flexural type plastic hinges were assumed to be inelastic sources for both beams and columns. Different methods for structural analysis were employed such as MRSA, NLSA and NLTH, assuming a comparable seismic demand. The obtained shear demands at joints were compared to shear strengths evaluated according to building codes targeted to existing structures. The following conclusions can be drawn:

1. The shear demand at a beam–column joint being a non-conventional output, a post-process based on nodal moments is needed. Two major hypotheses were made: (i) the internal lever arm at the column face cross section, of the beam, was assumed constant and (ii) the contribution to the horizontal equilibrium of the column's shear was neglected. The last assumption's results are conservative;
2. Shear strength evaluation should be extended to all the beam–column joints in a three-dimensional frame, distinguishing two flexural planes. Significant strength differences might be influenced by (i) the joint type attribute in each flexural plane and (ii) the use of different building codes;
3. The larger safety margin was recognized for corner joints by assigning to them the exterior joint type in both the flexural planes. Larger strength should be expected as a result of the confinement offered by the beams in both directions. Besides, elliptical strength interaction domain results were conservative when compared with NLTH shear demand orbits;
4. Among the reviewed building codes, EC8 produced larger strength predictions than ASCE41-17 and NZSEE2017. The latter produced the lowest ones. Discussion about the strength accuracy was not intended because the compared shear demands represent a condition far from failure;
5. NLSA was proven to estimate the larger shear demand with respect to MRSA and NLTH. Differences were explained as a consequence of the possible inaccuracy of NLSA, using modal combination, in the evaluation of elements' forces. Such evidence needs to be investigated further since NLSA is frequently adopted in the assessment of existing RC structures as a compromise between MRSA and NLTH.

Author Contributions: Conceptualization, A.M.; Methodology, A.M./G.M.; Software, A.M.; Validation, A.M.; Data Curation, A.M.; Writing—Original Draft and Reviews, A.M.; Writing—Reviews, G.M.; Supervision, G.M. All authors have read and agreed to the published version of the manuscript.

Funding: This research received no external funding.

Data Availability Statement: Data are available upon request.

Acknowledgments: Open access publication was financially supported by the Board of the PhD Programme of Structural, Seismic and Geotechnical Engineering at Politecnico di Milano.

Conflicts of Interest: The authors declare no conflict of interest.

Abbreviations

The following abbreviations are used in this manuscript:

CQC	Complete Quadratic Combination
dofs	degrees-of-freedom
MPA	Modal-pushover-Analysis
MRSA	Modal Response Spectrum
NLSA	Non-Linear Static Analysis

NLTH	Non-Linear Time History
PGA	Peak Ground Acceleration
PsD	Pseudo-dynamic
RC	Reinforced Concrete

References

- Varum, H. Seismic Assessment, Strengthening and Repair of Existing Buildings. Ph.D. Thesis, Universidade de Aveiro, Aveiro, Portugal, 2003.
- Kam, W.Y.; Pampanin, S.; Elwood, K. Seismic performance of reinforced concrete buildings in the 22 February Christchurch (Lyttelton) earthquake. *Bull. N. Z. Soc. Earthq. Eng.* **2011**, *44*, 239–278. [[CrossRef](#)]
- Pantazopoulou, S.; Bonacci, J. On earthquake-resistant reinforced concrete frame connections. *Can. J. Civ. Eng.* **1994**, *21*, 307–324. [[CrossRef](#)]
- Parate, K.; Kumar, R. Shear strength criteria for design of RC beam–column joints in building codes. *Bull. Earthq. Eng.* **2019**, *17*, 1407–1493. [[CrossRef](#)]
- Celik, O.C.; Ellingwood, B.R. Modeling beam–column joints in fragility assessment of gravity load designed reinforced concrete frames. *J. Earthq. Eng.* **2008**, *12*, 357–381. [[CrossRef](#)]
- Moehle, J.P. *Seismic Design of RC Buildings*; McGraw-Hill Education: New York, NY, USA, 2015. [[CrossRef](#)]
- Negro, P.; Fardis, M.N. *Seismic Performance Assessment and Rehabilitation of Existing Buildings (SPEAR) International Workshop Proceedings*; Office for Official Publication of the European Communities: Luxembourg, 2005.
- Paulay, T.; Priestley, N. *Seismic Design for Concrete and Masonry Buildings*; Wiley: New York, NY, USA, 1992.
- ACI. *ACI 318-19 Building Code Requirements for Structural Concrete and Commentary*; American Concrete Institute (ACI): Farmington Hills, MI, USA, 2019. [[CrossRef](#)]
- EN 1998-1:2004; Eurocode 8: Design of Structures for Earthquake Resistance. Part1: General Rules, Seismic Actions and Rules for Buildings. European Committee for Standardization (CEN): Brussels, Belgium, 2004.
- ACI 352R-02; Recommendations for Design of Beam-Column Connections in Monolithic Reinforced Concrete Structures (ACI-ASCE 352-02). American Concrete Institute (ACI): Farmington Hills, MI, USA, 2002.
- CEN/TC250/SC8; prEN1998-1-3:2022. Eurocode 8: Design of Structures for Earthquake Resistance. Part 1–3: Assessment and Retrofitting of Buildings and Bridges. European Committee for Standardization (CEN): Brussels, Belgium, 2004.
- NZSEE. *The Seismic Assessment of Existing Building*; Technical Report; New Zeland Society of Earthquake Engineering: Wellington, New Zealand, 2017.
- ASCE. *ASCE/SEI, 41-17 Seismic Evaluation and Retrofit of Existing Buildings*; American Society of Civil Engineers: Reston, VA, USA, 2017; p. 623.
- Oloukun, F.A. Prediction of concrete tensile strength from compressive strength: evaluation of existing relations for normal weight. *ACI Mater. J.* **1991**, *88*, 302–309.
- Hakuto, S.; Park, R.; Tanaka, H. Seismic Load Test on Interior and Exterior Beam-Column Joints with Substandards Reinforcing Details. *ACI J.* **2000**, *97*, 11–25.
- Kosmopoulos, A.; Fardis, M.N. Estimation of inelastic seismic deformations in asymmetric multistorey RC buildings. *Earthq. Eng. Struct. Dyn.* **2007**, *36*, 1209–1234. [[CrossRef](#)]
- Di Ludovico, M. Seismic Behavior of a Full-Scale RC Structure Retrofitted Using GFRP Laminates. *J. Struct. Eng.* **2008**, *134*, 810–821. [[CrossRef](#)]
- Negro, P.; Mola, E.; Molina, F.J.; Magonette, G.E. Full-scale PsD testing of a torsionally unbalanced three-storey non-seismic RC frame. In Proceedings of the 13th World Conference on Earthquake Engineering, Vancouver, BC, Canada, 1–6 August 2004; p. 968.
- Molina, F.J.; Negro, P. Bidirectional pseudodynamic technique for testing a three-storey reinforced concrete building. In Proceedings of the 13th World Conference on Earthquake Engineering, Vancouver, BC, Canada, 1–6 August 2004; p. 75.
- Reynouard, J.M.; Ile, N.; Brun, M. Inelastic seismic analysis of the SPEAR test building. *Eur. J. Environ. Civ. Eng.* **2010**, *14*, 855–867. [[CrossRef](#)]
- Bento, R.; Bhatt, C.; Pinho, R. Using nonlinear static procedures for seismic assessment of the 3D irregular SPEAR building. *Earthq. Struct.* **2010**, *1*, 177–195. [[CrossRef](#)]
- Freeman, S.A. Review of the Development of the Capacity Spectrum Method. *ISST J. Earthq. Technol.* **2004**, *41*, 113.
- Bhatt, C.; Bento, R. Extension of the CSM-FEMA440 to plan-asymmetric real building structures. *Earthq. Eng. Struct. Dyn.* **2010**, *40*, 1263–1282. [[CrossRef](#)]
- Combesure, A.; Gravouil, A. A numerical scheme to couple subdomains with different time-steps for predominantly linear transient analysis. *Comput. Methods Appl. Mech. Eng.* **2002**, *191*, 1129–1157. [[CrossRef](#)]
- Brun, M.; Batti, A.; Limam, A.; Combesure, A. Implicit/explicit multi-time step co-computations for predicting reinforced concrete structure response under earthquake loading. *Soil Dyn. Earthq. Eng.* **2012**, *33*, 19–37. [[CrossRef](#)]
- Di Ludovico, M. Comparative Assessment of Seismic Rehab Techniques on the Full Scale SPEAR Structure. Ph.D. Thesis, Università degli Studi di Napoli Federico II, Napoli, Italy, 2008.

28. Dolsek, M.; Fajfar, P. Simplified probabilistic seismic performance assessment of plan-asymmetric buildings. *Earthq. Eng. Struct. Dyn.* **2007**, *36*, 2021–2041. [[CrossRef](#)]
29. Fajfar, P. A Nonlinear Analysis Method for Performance-Based Seismic Design. *Earthq. Spectra* **2000**, *16*, 573–592. [[CrossRef](#)]
30. Fajfar, P.; Marušić, D.; Peruš, I. Torsional effects in the pushover-based seismic analysis of buildings. *J. Earthq. Eng.* **2005**, *9*, 831–854. [[CrossRef](#)]
31. Fajfar, P.; Marušić, D.; Peruš, I. The Extension of the N2 method to asymmetric buildings. In Proceedings of the 4th European Workshop on the Seismic Behaviour of Irregular and Complex Structures, Thessaloniki, Greece, 26–27 August 2005; p. 41.
32. Mola, E.; Negro, P.; Pinto, A. Evaluation of current approaches for the analysis and design of multi-storey torsionally unbalanced frames. In Proceedings of the 13th World Conference on Earthquake Engineering, Vancouver, BC, Canada, 1–6 August 2004; p. 3304.
33. Pardalopoulos, S.I.; Pantazopoulou, S.; Manolis, G.D. On the Modeling and Analysis of Brittle Failure in Existing RC Structures Due to Seismic Loads. *Appl. Sci.* **2022**, *12*, 1602. [[CrossRef](#)]
34. Rozman, M.; Fajfar, P. Seismic response of a RC frame building designed according to old and modern practices. *Bull. Earthq. Eng.* **2009**, *7*, 779–799. [[CrossRef](#)]
35. Stratan, A.; Fajfar, P. *Influence of Modelling Assumptions and Analysis Procedure on the Seismic Evaluation of Reinforced Concrete GLD Frames*; Technical Report; University of Ljubjana: Ljubjana, Slovenia, 2002.
36. Stratan, A.; Fajfar, P. *Seismic Assessment of the SPEAR Test Structure*; Technical Report January; University of Ljubljana: Ljubljana, Slovenia, 2003.
37. CSI. *CSI Analysis Reference Manual. For SAP2000, ETABS, SAFE, CsiBridge*; [Version 2013]; CSI: Berkeley, CA, USA, 2013.
38. Giberson, F. The Response of Non-Linear Multi-Story Structures Subjected to Earthquake Excitation. Ph.D. Thesis, California Institute of Technology, Pasadena, CA, USA, 1967.
39. Bentz, E.C. Sectional Analysis of Reinforced Concrete Members. Ph.D Thesis, University of Toronto, Toronto, ON, Canada, 2000.
40. FEMA. *FEMA 356 Seismic Rehabilitation of Buildings*; FEMA: Washington, DC, USA, 2000.
41. Takeda, T. Reinforced Concrete Response to Simulated Earthquakes. *J. Struct. Div.* **1970**, *96*, 19–26. [[CrossRef](#)]
42. Pantazopoulou, S.; French, C. Slab Participation in Practical Design of R.C. Frames. *ACI Struct. J.* **2001**, *98*, 479–489.
43. Birely, A.C.; Lowes, L.N.; Dawn, E.L. Linear analysis of concrete frames considering joint flexibility. *ACI Struct. J.* **2012**, *109*, 381–391. [[CrossRef](#)]
44. Fajfar, P.; Dolsek, M.; Marušić, D.; Stratan, A. Pre-and post-test mathematical modelling of the SPEAR building. In Proceedings of the SPEAR International Workshop Proceedings, Ispra, Italy, 4–5 April 2005; pp. 173–188.
45. Papazafeiropoulos, G.; Plevris, V. OpenSeismoMatlab: A new open-source software for strong ground motion data processing. *Heliyon* **2018**, *4*, e00784. [[CrossRef](#)]
46. Chopra, A.K.; Goel, R.K. A modal pushover analysis procedure to estimate seismic demands for unsymmetric-plan buildings. *Earthq. Eng. Struct. Dyn.* **2004**, *33*, 903–927. [[CrossRef](#)]
47. Newmark, N.M. Method of Computation for Structural Dynamics. *J. Eng. Mech. Div.* **1959**, *2*, 1235–1264. [[CrossRef](#)]
48. Shayanfar, J.; Bengar, H.A.; Parvin, A. Analytical prediction of seismic behavior of RC joints and columns under varying axial load. *Eng. Struct.* **2018**, *174*, 792–813. [[CrossRef](#)]
49. Bathe, K.J. *Finite Element Procedures*, 2nd ed.; K.J. Bathe: Watertown, MA, USA, 2006
50. Menun, C. Envelopes for seismic response vectors, I: Applications. *J. Struct. Eng.* **2000**, *126*, 474–481. [[CrossRef](#)]
51. Clough, R.W.; Penzien, J. *Dynamics of Structures*, 3rd ed.; Computers and Structures: Berkeley, CA, USA, 2003.
52. Kurose, Y.; Guimaraes, G.; Zuhua, L.; Kreger, M.; Jirsa, J.O. Evaluation of slab-beam-column connections subjected to bidirectional loading. *ACI Spec. Publ.* **1991**, *123*, 39–67.
53. Chopra, A.K.; Goel, R.K. A modal pushover analysis procedure for estimating seismic demands for buildings. *Earthq. Eng. Struct. Dyn.* **2002**, *31*, 561–582. [[CrossRef](#)]